

# Authors' Response to Reviewers' Comments

Manuscript No.: acp2018-1018, submitted to ACP

Title: Unravelling the microphysics of polar mesospheric cloud formation

Authors: D. Duft, M. Nachbar, T. Leisner

*The authors would like to thank the reviewers for taking the time to review the manuscript and for preparing detailed and helpful comments.*

## Anonymous Referee #1

*Received and published: 7 December 2018*

### Comment:

I have just seen the manuscript "The heterogeneous nature of polar mesospheric cloud formation" by Duft, Nachbar and Leisner (DNL). They report water uptake experiments on iron-silicate nanoparticles for various particles sizes and water supersaturation ratios at 128-152 K. This manuscript is part of a series of works by the same three authors - three manuscripts were published in 2016 and 2018, and two manuscripts are reported as submitted. The latter were not available to me at the time of this review.

### Reply:

Much to the authors regret, one of the two mentioned manuscripts was accepted and published online one week after initial submission of this manuscript (Nachbar et al., 2018c). It was, however, available after the referee quick reports and before the final manuscript was uploaded for the open discussion. In the uploaded open discussion manuscript the publication is cited with a complete and updated reference. The second submitted manuscript mentioned (Nachbar et al., 2018d) is of minor importance for the results and conclusions of the current manuscript as we only refer to it as an accompanying article in the final paragraph. This manuscript was available as a discussion paper on ACPD before the beginning of the open discussion.

### Comment:

The main conclusion is that noctilucent clouds may form under the experimental conditions in the mesosphere below supersaturations that are typically observed in Earth's upper atmosphere. A secondary conclusion that has already been reported in their earlier manuscripts is that amorphous solid water (ASW) rather than crystalline ice I (cubic, hexagonal or stacking-disordered) condenses on such smoke particles. Finally, they claim that charge effects or sunlight absorption by the particles is of minor relevance for the formation of mesospheric clouds. An impressive number of almost 200 experiments under different conditions has been performed. However, the data themselves are not convincing, and I have also doubts about the model used to interpret the data as detailed below:

### Remark:

The following major concerns by the referee do not question the experimental results on the critical saturation. Rather, the critique is directed at the modelling part.

### Comment:

1) My major concern is on the nature of the condensed ASW. The authors treat ASW as if it was a well-defined phase, just like a crystalline phase. However, it is well known that the nature of ASW deposits differs very much depending on the growth conditions. ASW is usually a highly microporous materials. Porosities can be close to 0 or up to 80%, specific surface areas can be between almost 0 and several hundred m<sup>2</sup>/g. Furthermore, ASW is well known to take up background gases very

efficiently and incorporate them into its pores, burying them into its bulk. In fact, some of the micropores in ASW are large enough to take up the whole iron-silicate particle of length scale 1-3 nm in a single pore. Some of this is described by Kay and co-workers (Science 283 1999) as well as by Mayer and Pletzer (J. Phys. Colloques 48 1987 and Nature 319 1986). Unfortunately, any kind of characterization of the ASW particles in terms of porosities, uptake of background gas or additional Fe-Si nanoparticles is missing in this work. Still the authors use specific values in their modelling, e.g., a density of 0.93 g/ml in order to determine the water coverage and wet particle radius. How would the model be affected if the density was much lower than that because of a high porosity within ASW?

**Reply:**

The authors agree with the referee that ASW in general is not a well-defined phase as it may be produced in a wide range of experimental growth conditions. It is well known that depending on growth conditions microporous ASW may be formed and that background gas molecules may be trapped if the gas is present during deposition. The most critical parameters for the creation of microporous ASW appear to be deposition angle, deposition rate and substrate temperature (Dohnalek et al., 2003; Hill et al., 2016; Kimmel et al., 2001; Kouchi et al., 1994; Mayer and Pletzer, 1986; Mitterdorfer et al., 2014; Raut et al., 2007; Stevenson et al., 1999). However, highly porous ASW was usually produced using surface temperatures below 77K. ASW samples that were prepared by deposition at surface temperatures between 90 and 110K revealed either only a small degree of porosity (Brown et al., 1996; Chonde et al., 2006), or were nonporous (Kimmel et al., 2001; Stevenson et al., 1999). ASW samples produced above 110K in the absence of a background gas were found to be compact or exhibited the same surface area (determined by gas adsorption experiments) as crystalline ice reference samples indicating the formation of compact ASW (Mayer and Pletzer, 1986; Stevenson et al., 1999; Westley et al., 1998). We thus argue that at the experimental conditions employed in our study (surface temperature of  $T \geq 128\text{K}$ , maximum deposition rate  $3\text{\AA}/\text{s}$  ( $\sim 1\text{ML}/\text{s}$ ), Helium as a background gas) compact ASW is created with at maximum a marginal degree of porosity. Based on the results of the cited studies we believe that compact ASW can be regarded as a well-defined phase and that it is justified to use specific (temperature-dependent) values for e.g. the density, the vapour pressure, or the surface tension of compact ASW.

**Changes made:**

To address the apparent potential for ambiguity between 'ASW in general' and 'compact ASW', we updated the manuscript and replaced 'ASW' with 'compact ASW' where appropriate. We also added a clarifying statement to section 3.2 (page 9 lines 4-10).

**Comment:**

Even more troublesome is the saturation water vapor of ASW ( $S_{\text{ASW}}$ ) used in equation (1) of the model. The vapour pressure of ASW maybe much smaller than the one parameterized by Nachbar et al. due to the incorporation of foreign atoms/molecules into the ASW matrix - which automatically implies that the supersaturations given by DNL may be very different from what they assume in their model. Also the internal porosity and surface corrugation may have a large impact on the vapor pressure. No critical analysis with respect to these uncertainties is discussed in their model. The values they have chosen seem to be taken as granted and are not critically discussed or given the possibility for a range of values for different individual ASW particles - in particular there is no analysis how the results would change if  $S_{\text{ASW}}$  and the density were different.

**Reply:**

We agree with the referee that the assumption of porous ice with possible incorporation of foreign atoms would render the model inconclusive as large uncertainties in ice density, vapour pressure and surface tension are linked with this assumption. For instance, the surface area as well as the vapour

pressure were found to vary by a factor as large as 10 depending on growth conditions (e.g. Kouchi, 1987; Mayer and Pletzer, 1986; to name just two studies).

However, and as already detailed above, the authors have no indication to assume that the ice formed under the experimental conditions is either porous or has significant amounts of foreign atoms incorporated.

Additionally, the model provides an excellent representation of the experimental data (compare Fig. 6). The standard deviation between model and experimental data including all data points shown is only 9%. The authors would like to emphasize that the model is based on only two main quantities: 1) on a parameterization for the water coverage at mesopause conditions which is based on experimental data shown in this manuscript, and 2) on the Kelvin-Thomson equation in which we use the available specific values for compact ASW. These two quantities alone are sufficient to reproduce measured critical saturations for nanoparticle radii ranging from 1 to 2.8nm, at temperatures between 128 and 147K, H<sub>2</sub>O vapour pressures in the range between about  $2 \times 10^{-7}$  to  $7 \times 10^{-5}$ Pa, and covering different iron-silicate compositions. The striking agreement and the simplicity of the model is a compelling support for the model including the underlying assumptions.

**Comment:**

2) The data themselves show a very large scatter. For example in Fig.3 the desorption energies for the SiO<sub>2</sub> nanoparticles in the range of 0.3-0.5 nm<sup>-1</sup> scatter more or less randomly between 38.5 and 40.0 kJ/mol. With equal justification one could fit a line independent of particle size or that even shows larger desorption energies for smaller particles. The fit given by DNL hinges mainly on the 4 data points between 0.5 and 0.7 nm<sup>-1</sup>, whereas the other roughly 40 data points do not show any trend. That is, there is a large uncertainty associated with the size-dependent desorption energies deduced from Fig.3 that is not at all reflected in the error-bars in Fig.4. Why is the error-bar for the curvature-independent desorption energy for SiO<sub>2</sub> and Fe<sub>2</sub>O<sub>3</sub> in Fig.4 of similar size, even though the data points for Fe<sub>2</sub>O<sub>3</sub> particles scatter much less around the fitted line? A problem that goes hand in hand with this inappropriate fit is the surface-tension deduced from the slope in Fig.3: why is the surface tension for SiO<sub>2</sub> half of the one found for Fe<sub>2</sub>O<sub>3</sub> or Fe<sub>65</sub>Si<sub>35</sub>O<sub>300</sub>? One would expect very similar values for all three types of nanoparticles - which demonstrates that the values deduced from Fig.3 are associated with a huge error, much larger than the "+/- 18 mN/M" given by DNL. In my opinion the data for SiO<sub>2</sub> do not even allow to exclude a surface tension below 0.

**Reply:**

The authors did not follow an arbitrary procedure when fitting the data shown in Fig. 3 but instead used the basic linear regression function which is implemented in the graphical analysis software OriginPro 2018b by OriginLab Corporation. The employed linear regression algorithm is well documented (URL: <https://www.originlab.com/doc/Origin-Help/LR-Algorithm> ; last access 23 January 2019) as well as the method for calculating the standard errors of the fit parameters. In the manuscript the authors report the values as retrieved from the analysis software. The fact, that the experimental data for E<sub>des</sub> of the SiO<sub>2</sub> particles shown in Fig. 3 is not strongly correlated with the inverse particle radius is directly reflected by the high standard error of the fitted slope for the SiO<sub>2</sub> particles. Ultimately, and as stated in the manuscript, a combined fit for all three materials is performed to avoid using a material dependent surface tension for the water ad-layer in Eq. 5. This procedure will result in a single value for the surface tension for the three materials but ignores the possibility that the surface tension of the thin water ad-layer - air interface may be substrate dependent. However, as we show later in the manuscript, this approach is a good simplification for modelling the water coverage. The results in Fig. 5 show that using this procedure we are able to predict the water coverage sufficiently well. Nevertheless, the authors are aware that the model is not fully able to reproduce the variation in measured water coverage. This may hint to possible

deficiencies in the parameterization or to other unknown parameters influencing the water coverage.

The authors agree with the referee that the error bars for the SiO<sub>2</sub> data point in Fig. 4 do not reflect the error in the intercept in Fig. 3 when fitting the SiO<sub>2</sub> data alone. The error bars in Fig. 4 represent the standard error for the intercept from the combined fit, which implicitly assumes that the slope is identical for all three materials. In the combined fit all data points from the three materials contribute equally with the result that the large quantity of iron oxide data points dominates the final fitted slope and standard error. We believe that the error bars in Fig. 4 are correct under the assumption of a constant surface tension for all three materials.

**Changes made:**

We adapted the caption of Fig. 3 to be more precise.

**Comment:**

Similarly, also in Fig.5 the scatter of the data is unacceptably large. I believe this huge scatter reflects that  $S_{ASW}$  cannot be defined in the straightforward way assumed by DNL. In fact,  $S_{ASW}$  needs to be defined individually for each particle, depending on density, curvature and porosity of each deposit. This task is obviously unfeasible, but this still does not validate the use of an invalid assumption.

**Reply:**

The authors do not agree that the error bars in Fig. 5 are unacceptably large. As stated in the manuscript, calculated and measured water coverages deviate on average by 7% with a mean square deviation of 22%. The authors would like to remind the reader that the presented parameterization covers particle radii ranging from 1 to 3nm, temperatures between 128 and 152K, H<sub>2</sub>O vapour pressures between  $2 \times 10^{-7}$  and  $1 \times 10^{-4}$ Pa, and different iron-silicate compositions. The parameterization is intended to be used as a predictor for the water coverage on small iron-silicate nanoparticles in the highly variable environment of the polar mesosphere. In this context the authors believe that this deviation is more than acceptable.

**Comment:**

3) I did not understand from this manuscript why the authors believe that charges do not play a role. Which experimental finding allows for this statement? This needs to be elaborated.

**Reply:**

In the abstract, results and discussion, and conclusion sections the authors state: “[...] *charge effects play only a minor role in NLC formation for particles larger than a dry size of  $r=0.6\text{nm}$ .*”

We agree with the referee that in the manuscript no experimental data for the critical saturation of uncharged particles is presented as proof for the above statement. Instead, only measurements of the activation of ice growth on nanoparticles carrying a single positive charge are presented. However, the authors also present an ice activation model intended to predict critical ice growth conditions. The model is very simple as it is based on the Kelvin-Thomson equation for the wet particle diameter, which is the generalized Kelvin equation for charged liquid particles. Except for the parameterization of the water coverage, no further fitting procedure was employed in the model. As shown in Fig. 6, the experimental data is reproduced excellently by this simple model. The authors interpret this as a strong indication that ice activation under these conditions is governed by the basic energetic principles underlying the Kelvin-Thomson equation.

In the manuscript, the authors expand this interpretation by investigating the influence of the particle charge in the Kelvin-Thomson equation. Comparison of the dash-dotted and solid curves in

Fig. 8b which were obtained by setting  $Q=1e$  and  $Q=0e$  in their model shows that *in their model* the critical saturation is only marginally influenced by the single charge residing on the particle. It is thus from the model results that we draw this conclusion about “the minor role of charge effects”. We agree that in the manuscript the basis for the authors’ conclusion on the charge effect is not made sufficiently clear. We therefore modified and adapted the relevant paragraphs as follows:

**Changes made:**

abstract section, page 1, lines 15+

results section, page 11, line 24

conclusion section, page 12, lines 11-13

**Remark:**

While reviewing the corresponding figures and paragraphs concerning the influence of the particle charge we discovered that in Fig. 8b, instead of the model of Yu (2005), the model by Lapshin et al. (2002) was used. We updated Fig. 8 and included the result of our ice activation model using the modified Kelvin-Thomson formulation by Yu (2005) while keeping the result obtained using the model introduced by Lapshin and co-workers.

**Changes made:**

Included an additional model curve in Fig. 8b. Corrected labels, caption and text related to Fig 8b.

**Comment:**

Even though the mesosphere contains mostly positively charged ions such as  $N_2^+$ ,  $NO^+$ ,  $O_2^+$ ,... I would also be interested to see what role negative ions (electrons) might play. Can the authors rule out an influence of electrons on the formation of noctilucent clouds?

**Reply:**

Regarding the polarity of the particle charge the authors note that in the Kelvin-Thomson equation the particle charge enters as  $Q^2$ . Hence, in the authors’ model the sign of the particle charge does not play a role.

Furthermore, application of the Kelvin-Thomson equation using bulk properties is at least questionable for very small particles in the cluster size regime. The authors therefore cannot rule out an influence of molecular ions or electrons on NLC formation on the basis of the experimental data or the ice activation model as presented in this manuscript.

**Comment:**

As the manuscript stands now, I do not feel that it reports important new physics or chemistry that goes beyond what DNL have published in their recent papers on this topic. The manuscript needs to take into account uncertainties in the model and the nature of the formed ASW with much more care.

**Reply:**

In the manuscript under review, the authors present laboratory experimental data on the critical saturation for ice growth on small nm-sized meteoric smoke analogue particles at conditions similar to those in the polar summer mesopause. The manuscript constitutes the first report on such measurements and the results are direct proof that heterogeneous formation on small nanoparticles is possible at typical mesopause conditions. This result is a strong indication that indeed meteoric smoke particles are the origin for ice particle formation in the mesopause. This in turn strengthens the modelling of NLC formation which heavily depends on the knowledge of the mechanism and the conditions under which ice particle formation may take place in NLCs. The authors believe that the results presented in this manuscript constitute a major advancement in the understanding of ice

formation in the mesopause. The manuscript clearly goes beyond our recent publications, which are 1) on the water affinity and mixing state of iron silicate nanoparticles produced in our setup (Nachbar et al., 2018a), 2) on the vapour pressure of nano-crystalline ice (Nachbar et al., 2018b), and 3) on the vapour pressure of (compact) ASW (Nachbar et al., 2018c).

The authors therefore feel justified to not agree with the referee on this particular comment.

## **Anonymous Referee #2**

*Received and published: 5 December 2018*

### **Comment:**

This is a very important study. It shows - for the first time - that H<sub>2</sub>O ice will form on metal silicate particles smaller than 2 nm in radius, at H<sub>2</sub>O supersaturations that are regularly encountered in the upper mesosphere at high latitudes during summer. The study therefore answers a long-running problem: what is the source of the nuclei for polar mesospheric clouds. The work also shows that the metal oxide/silicate particles do not need to be charged to act as effective ice nuclei under these conditions.

The paper describes a beautiful experimental study, carefully carried out. The precision is such that the authors are able to derive three equations (6, 7 and 10), which determine the ice cloud activation threshold as a function of humidity and temperature, as well as the radius and iron content of the nucleating particle. This is exactly what modellers need to predict where and when these clouds will form, and hence to understand their relevance as a marker for climate change in the middle atmosphere. The authors are to be congratulated on their achievement.

The paper is clearly written and illustrated, and I have only a few grammatical corrections and other minor suggestions which are listed below.

p. 1, line 12: "We observe that ice growth ..." i.e. remove the comma

corrected

p. 1, line 13: define NLC

replaced "NLC" with "polar mesospheric cloud"

p. 1, line 25: space-borne

corrected

p. 2, line 10: "Model simulations have shown that ..." i.e. remove the comma

corrected

p. 4, line 13: the method used to estimate the number of monolayers is described in the next section, and should be referred to here e.g. "(see Section 3.1 for method of calculating layer thickness)"

suggestion adopted

p. 6, line 3: "we assume is similar..."

corrected

p. 7, line 5: " in Nachbar et al. (2018a) ..."

corrected. We also noticed that in this paragraph we incorrectly refer to “the surface tension of ASW” when actually it should read “the surface tension of supercooled liquid water”. We changed the statement and the subscripts in the in-line formula accordingly.

p. 11, line 21: perhaps you could suggest here why there is this disagreement?

At the moment, we can only speculate on the reasons for this disagreement. There might be an error involved in the mathematical derivation of the model by Lapshin et al. while we suspect that the ion-dipole interaction is not correctly implemented in both models, by Lapshin et al. and by Yu, respectively. Review of these hypotheses goes beyond the scope of this manuscript and remains as a subject for future investigations.

#### **Changes made:**

Replaced “equilibrium saturation” with “critical saturation” in the paragraph starting at line 21 on page 11 for consistency with the rest of the manuscript.

p. 12, line 9: "Our findings show that due ..." i.e. remove the comma and "that"

corrected

#### **References**

- Brown, D. E., George, S. M., Huang, C., Wong, E. K. L., Rider, K. B., Smith, R. S., and Kay, B. D.: H<sub>2</sub>O Condensation Coefficient and Refractive Index for Vapor-Deposited Ice from Molecular Beam and Optical Interference Measurements, *J. Phys. Chem.*, 100, 4988-4995, doi: 10.1021/jp952547j, 1996.
- Chonde, M., Brindza, M., and Sadtchenko, V.: Glass transition in pure and doped amorphous solid water: An ultrafast microcalorimetry study, *J. Chem. Phys.*, 125, 094501, doi: 10.1063/1.2338524, 2006.
- Dohnalek, Z., Kimmel, G. A., Ayotte, P., Smith, R. S., and Kay, B. D.: The deposition angle-dependent density of amorphous solid water films, *J. Chem. Phys.*, 118, 364-372, doi: 10.1063/1.1525805, 2003.
- Hill, C. R., Mitterdorfer, C., Youngs, T. G. A., Bowron, D. T., Fraser, H. J., and Loerting, T.: Neutron Scattering Analysis of Water's Glass Transition and Micropore Collapse in Amorphous Solid Water, *Phys. Rev. Lett.*, 116, 5, doi: 10.1103/PhysRevLett.116.215501, 2016.
- Kimmel, G. A., Stevenson, K. P., Dohnalek, Z., Smith, R. S., and Kay, B. D.: Control of amorphous solid water morphology using molecular beams. I. Experimental results, *J. Chem. Phys.*, 114, 5284-5294, doi: 10.1063/1.1350580, 2001.
- Kouchi, A.: Vapour pressure of amorphous H<sub>2</sub>O ice and its astrophysical implications, *Nature*, 330, 550, doi: 10.1038/330550a0, 1987.
- Kouchi, A., Yamamoto, T., Kozasa, T., Kuroda, T., and Greenberg, J. M.: Conditions for condensation and preservation of amorphous ice and crystallinity of astrophysical ices, *Astron. Astrophys.*, 290, 1009-1018, 1994.
- Lapshin, V. B., Yablokov, M. Y., and Palei, A. A.: Vapor pressure over a charged drop, *Russ. J. Phys. Chem.*, 76, 1727-1729, 2002.
- Mayer, E. and Pletzer, R.: Astrophysical implications of amorphous ice - a microporous solid, *Nature*, 319, 298-301, doi: 10.1038/319298a0, 1986.

- Mitterdorfer, C., Bauer, M., Youngs, T. G. A., Bowron, D. T., Hill, C. R., Fraser, H. J., Finney, J. L., and Loerting, T.: Small-angle neutron scattering study of micropore collapse in amorphous solid water, *Phys. Chem. Chem. Phys.*, 16, 16013-16020, doi: 10.1039/c4cp00593g, 2014.
- Nachbar, M., Duft, D., Kiselev, A., and Leisner, T.: Composition, Mixing State and Water Affinity of Meteoric Smoke Analogue Nanoparticles Produced in a Non-Thermal Microwave Plasma Source, *Z. Phys. Chem.*, 232, 635-648, doi: 10.1515/zpch-2017-1053, 2018a.
- Nachbar, M., Duft, D., and Leisner, T.: The vapour pressure over nano-crystalline ice, *Atmos. Chem. Phys.*, 18, 3419-3431, doi: 10.5194/acp-18-3419-2018, 2018b.
- Nachbar, M., Duft, D., and Leisner, T.: Volatility of Amorphous Solid Water, *J. Phys. Chem. B*, 122, 10044-10050, doi: 10.1021/acs.jpcc.8b06387, 2018c.
- Nachbar, M., Wilms, H., Duft, D., Aylett, T., Kitajima, K., Majima, T., Plane, J. M. C., Rapp, M., and Leisner, T.: The impact of solar radiation on polar mesospheric ice particle formation, *Atmos. Chem. Phys. Discuss.*, 2018, 1--13, doi: 10.5194/acp-2018-1032, 2018d.
- Raut, U., Fama, M., Teolis, B. D., and Baragiola, R. A.: Characterization of porosity in vapor-deposited amorphous solid water from methane adsorption, *J. Chem. Phys.*, 127, 6, doi: 10.1063/1.2796166, 2007.
- Stevenson, K. P., Kimmel, G. A., Dohnalek, Z., Smith, R. S., and Kay, B. D.: Controlling the morphology of amorphous solid water, *Science*, 283, 1505-1507, doi: 10.1126/science.283.5407.1505, 1999.
- Westley, M. S., Baratta, G. A., and Baragiola, R. A.: Density and index of refraction of water ice films vapor deposited at low temperatures, *J. Chem. Phys.*, 108, 3321-3326, doi: 10.1063/1.475730, 1998.
- Yu, F.: Modified Kelvin–Thomson equation considering ion-dipole interaction: Comparison with observed ion-clustering enthalpies and entropies, *J. Chem. Phys.*, 122, 084503, doi: 10.1063/1.1845395, 2005.

# Unravelling the microphysics of polar mesospheric cloud formation

Denis Duft<sup>1</sup>, Mario Nachbar<sup>1</sup>, Thomas Leisner<sup>1,2</sup>

<sup>1</sup> Institute of Meteorology and Climate Research, Karlsruhe Institute of Technology, Karlsruhe, 76021, Germany

<sup>2</sup> Institute of Environmental Physics, University of Heidelberg, Heidelberg, 69120, Germany

5 *Correspondence to:* Denis Duft (denis.duft@kit.edu)

**Abstract.** Polar mesospheric clouds are the highest water ice clouds occurring in the terrestrial atmosphere. They form in the polar summer mesopause, the coldest region in the atmosphere. It has long been assumed that these clouds form by heterogeneous nucleation on meteoric smoke particles which are the remnants of material ablated from meteoroids in the upper atmosphere. However, until now little was known about the properties of these nm-size particles and application of the classical theory for heterogeneous ice nucleation was impacted by large uncertainties. In this work, we performed laboratory measurements on the heterogeneous ice formation process at mesopause conditions on small ( $r=1$  to 3 nm) iron-silicate nano-particles serving as meteoric smoke analogues. We observe that ice growth on these particles sets in for saturation ratios with respect to hexagonal ice below  $S_h=50$ , a value that is commonly exceeded during polar mesospheric cloud season, affirming meteoric smoke particles as likely nuclei for heterogeneous ice formation in mesospheric clouds. We present a simple ice activation model based on the Kelvin-Thomson equation that takes into account the water coverage of iron-silicates of various compositions. The activation model reproduces the experimental data very well using bulk properties of compact amorphous solid water. This is in line with the finding from our previous study that ice formation on iron-silicate nano-particles occurs by condensation of amorphous solid water rather than by nucleation of crystalline ice at mesopause conditions. Using the activation model, we also show that for iron-silicate particles with dry radius larger than  $r=0.6$  nm the nano-particle charge has no significant effect on the ice activation threshold.

## 1 Introduction

Polar mesospheric clouds (PMC) are water ice clouds occurring in the terrestrial atmosphere at an altitude of about 83 km (e.g. Rapp and Thomas, 2006; Thomas, 1991; Thomas and Olivero, 2001). The clouds form during the polar summer in the mesopause and have been reported in the literature for the first time at the end of the 19<sup>th</sup> century (Leslie, 1885). They are optically very thin and can be seen from ground by the naked eye only after the sun has set below the horizon, which is why they are often called noctilucent clouds (NLC). In recent years NLCs have been intensely studied using ground-based (e.g. Demissie et al., 2014; Kaifler et al., 2013; Kirkwood et al., 2008) and space-borne (e.g. DeLand et al., 2007; Hervig et al., 2016; Rong et al., 2015) methods. Additional studies have shown that during NLC season local temperatures are highly variable with mean temperatures of about 140 K and extremes as low as 100 K (Lübken et al., 2009; Rapp et al., 2002). Typical H<sub>2</sub>O concentrations of a few parts per million (Hervig et al., 2009; Seele and Hartogh, 1999) then lead to highly

supersaturated conditions, i.e. saturation ratios exceeding  $S_h=100$  are frequently observed (Lübken et al., 2009). It is commonly believed that such high supersaturations in the summer mesopause initiate the heterogeneous formation of crystalline ice on meteoric smoke particles (MSP) (Gumbel and Megner, 2009; Keese, 1989; Rapp and Thomas, 2006). MSPs are nano-particles which form by re-condensation of material ablated from meteoroids entering the upper atmosphere (Plane et al., 2015). Recent studies estimated that about 40 t of cosmic material enter the atmosphere each day (Carrillo-Sánchez et al., 2016; Hervig et al., 2017). Approximately 20 % of this material ablates in the upper atmosphere with the major elemental species being Fe, Mg, and Si (Vondrak et al., 2008). The ablated elemental species then form oxide-, hydroxide-, and carbonate compounds below 85 km and polymerize into nanometer-sized particles (Plane et al., 2015), which are likely present in the form of magnetite ( $\text{Fe}_3\text{O}_4$ ), wüstite ( $\text{FeO}$ ), magnesiowüstite ( $\text{Mg}_x\text{Fe}_{1-x}\text{O}$ ,  $x=0-0.6$ ), or iron-rich olivine ( $\text{Mg}_{2x}\text{Fe}_{2-2x}\text{SiO}_4$ ,  $x=0.4-0.5$ ) (Hervig et al., 2017; Rapp et al., 2012). Strong atmospheric circulation limits the average lifetime of these particles in the summer mesopause such that they only reach sizes below about  $r=2$  nm (Bardeen et al., 2008; Megner et al., 2008a; Megner et al., 2008b; Plane et al., 2014). Model simulations have shown that about 10 % of these particles are negatively charged at NLC height and season (Plane et al., 2015; Plane et al., 2014).

Precise modelling of the formation process of NLCs is, however, hindered by a limited understanding of the microphysical processes involved in heterogeneous ice formation under mesopause conditions. Here, the main unknown parameters are the surface properties of MSPs (i.e. the ability of the material to serve as ice nuclei), the ice phase forming at mesopause conditions, and the effect the electrical charge of MSPs may have on the ice formation process. In order to improve our understanding of NLC formation we recently introduced an experimental setup to study ice formation and growth processes on nano-particles exposed to realistic mesopause conditions (Duft et al., 2015). We used this setup in two previous studies to investigate ice growth rates on iron-oxide and silica nano-particles which served as analogues for MSPs (Nachbar et al., 2018b, c). We demonstrated that water vapour condenses in the form of compact amorphous solid water (ASW) at temperatures of the summer mesopause. In this study we follow up on our recent work and precisely measure onset conditions for the activation of ice growth on small meteoric smoke particle analogues at PMC formation conditions. We performed laboratory experiments by choosing conditions with saturation ratios below and above the activation threshold for ice growth. From these experiments, we determined critical saturations  $S_{\text{crit}}$  needed to activate ice growth. We analysed the data considering the formation of ASW and present a new adsorption-activation model, which highly reduces the current uncertainties in describing ice particle formation in the mesopause.

## 2 Methods

In this work we performed laboratory experiments using the MICE-TRAPS apparatus which was described earlier (Duft et al., 2015; Meinen et al., 2010; Nachbar et al., 2018b; Nachbar et al., 2016). In brief, sub-4nm iron-silicate nano-particles of adjustable elemental composition are produced in a microwave plasma particle source as MSP analogues (Nachbar et al., 2018a). The nano-particles are transferred continuously to the low pressure ( $p<10^{-4}$  mbar) Trapped Reactive Atmospheric

Particle Spectrometer (TRAPS) by means of an aerodynamic lens system. Within TRAPS the nano-particles carrying a single positive charge are mass-selected and levitated in the Molecular flow Ice Cell (MICE). MICE is a combination of a linear quadrupole ion trap and a water vapour supersaturation cell in which pressure, temperature, and humidity conditions of the polar summer mesopause can be established. The nano-particles trapped in MICE are thermalized by collisions with a He background gas. The water vapour partial pressure in MICE is set by temperature controlled sublimation from ice covered surfaces which have been installed in addition to the ion trap electrodes. In this work, the saturation ratio  $S$  (short: saturation) is usually given with respect to the saturation vapour pressure of compact ASW ( $S_{ASW}$ ). In some cases, and in order to facilitate comparison with previous studies, the saturation ratio is also given with respect to the saturation vapour pressure of hexagonal ice ( $S_h$ ), for which we use the well-established parameterization given by Murphy and Koop (2005). The saturation  $S_{ASW}$  can be obtained from  $S_h$  using the following relation (Nachbar et al., 2018c):

$$\frac{S_h}{S_{ASW}} = \frac{p_{sat,ASW}}{p_{sat,h}} = \exp\left(\frac{2312 [Jmol^{-1}] - 1.6 [Jmol^{-1}K^{-1}] \cdot T}{RT}\right). \quad (1)$$

We use the terms supersaturation and supersaturated conditions for cases in which the saturation is larger than 1.

A typical experiment in MICE starts by filling the particle trap with about  $10^7$  size-selected, singly-charged nano-particles in about 1s. Water adsorption and condensation on the trapped nano-particles is monitored by periodically extracting small fractions of the trapped nano-particle population and measuring the nano-particle mass as a function of the trapping time using a time-of-flight mass spectrometer. The saturation is usually varied by changing the particle temperature while keeping the water vapour density in MICE constant to facilitate comparison. In principle, water vapour density and particle temperature can be chosen independently within the limits of this experimental approach (Duft et al., 2015). Typical mass growth curves of iron oxide particles of initial radius  $r_{dry}=1.87$  nm are shown in Fig. 1 for various water vapour saturation ratios between  $S_{ASW}=1.4$  and  $S_{ASW}=16$ .

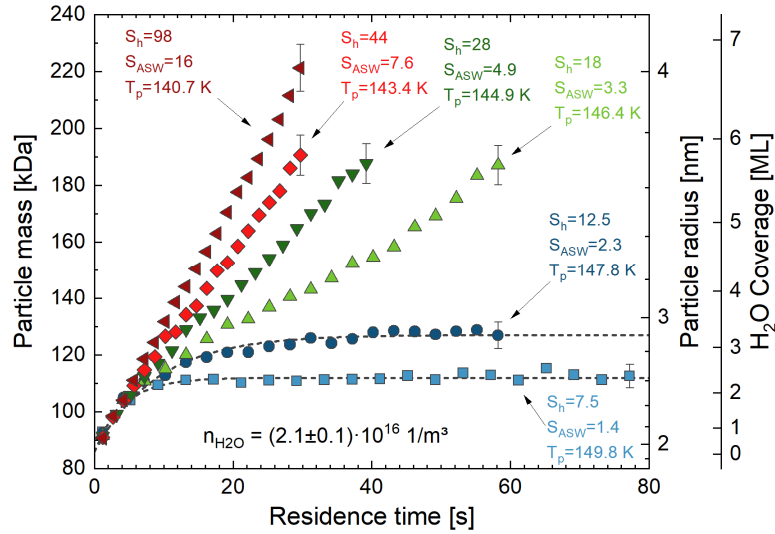


**Figure 1. Water vapour adsorption and depositional growth on Fe<sub>2</sub>O<sub>3</sub> nano-particles of initial radius  $r_{dry}=1.87$  nm under supersaturated conditions. Particle temperature varied between  $T=140.7$  K at  $S_{ASW}=16$  and  $T=149.8$  K at  $S_{ASW}=1.4$ . Typical error bars are shown for the last point of each series.**

We note that mass growth occurs independent of the saturation within the first few seconds when using a fixed water vapour concentration. At longer residence times two distinct regimes can be identified:

At low supersaturation ( $S_{ASW}=1.4$  and  $S_{ASW}=2.3$ ) the particle mass growth rate decreases with time after the initial growth. The mass accretion due to water adsorption is compensated by an increasing mass loss due to desorption from the particle surface. The particle mass then approaches a steady equilibrium state after about 25 s for the case shown. This behaviour is observed for all saturation ratios below a certain critical saturation threshold. In the following we will refer to the saturation regime below the critical threshold (i.e. in which the particle mass reaches a steady state) as the equilibrium regime. The mass of adsorbed water molecules  $m_{ads}$  in the steady state can be determined by fitting a simple exponential function of the following form to the data

$$m(t) = m_0 + m_{ads}(1 - \exp(-t/\tau)) . \quad (2)$$

Here,  $m$  is the particle mass as function of the residence time  $t$ ,  $m_0$  is the initial particle mass, and  $\tau$  is the characteristic time for reaching the steady state. Fits of Eq. (2) to the data for  $S_{ASW}=1.4$  and  $S_{ASW}=2.3$  are shown by the black dashed curves in Fig. 1 resulting in  $m_{ads}=26$  kDa and  $m_{ads}=41$  kDa, respectively. These values for  $m_{ads}$  correspond to 2.3 and 3.2 monolayers of adsorbed water which significantly increases the size of the nano-particles. A parameterization describing the amount of adsorbed water in equilibrium regime and the method of calculating layer thickness from measured adsorbed water mass are described in Sect. 3.1.

At higher supersaturation ( $S_{ASW}=3.3$  and above) a continuous particle growth is observed. In this growth regime, condensation always exceeds evaporation from the particle surface. The critical saturation for activation of ice growth  $S_{crit}$  is obtained in the experiment by monitoring the conditions at which the transition between equilibrium regime and growth regime occurs (i.e. between  $S_{ASW}=2.3$  and  $S_{ASW}=3.3$  in Fig. 1). By choosing finer temperature steps the critical saturation can be determined with higher accuracy. Measured critical saturations will be presented in Sect. 3.2 together with an ice activation model which describes the measured data.

### 3 Results and Discussion

#### 3.1 Adsorption in the equilibrium regime

In this section we present a parameterization for the water coverage on iron silicate particles at mesospheric conditions. Traditionally, the amount of water vapour adsorbed on a surface is described using adsorption isotherms where the water coverage is plotted as function of the saturation ratio (e.g. Venables et al., 1984). The water coverage  $\Theta$  is defined as the number of adsorbed water monolayers and is calculated using the wet and dry particle radius as  $\Theta=(r_{wet}-r_{dry})/d_{ML}$ . For  $d_{ML}$  we use the average distance of water molecules in the condensed state  $d_{ML}=(m_{H_2O}/\rho)^{1/3}$  with molecular mass  $m_{H_2O}$  and the

density of ice ( $\rho=930 \text{ kg m}^{-3}$ ). For hydrophilic materials as iron-oxides and silica it is known that multilayer adsorption occurs (Mazeina and Navrotsky, 2007; Navrotsky et al., 2008; Sneh et al., 1996).

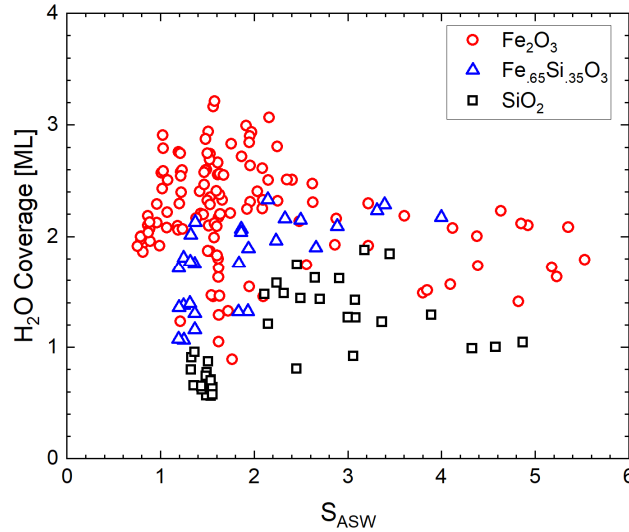


**Figure 2. Water coverage on iron-silicate nano-particles as a function of saturation.**

- 5 We measured the mass of adsorbed water vapour in equilibrium regime for iron oxide, silica and mixed iron silicate particles ( $r_{\text{dry}}=1.05 - 3.05 \text{ nm}$ ) covering the temperature range between 128 and 152 K in a total of 192 experiments. We converted the measured adsorbed mass to  $\text{H}_2\text{O}$  coverages and plot the results in Fig. 2 as a function of  $S_{\text{ASW}}$ . The coverage on iron oxide particles is typically higher compared to iron-silicate and silica particles which is in line with measurements showing that iron oxide exhibits a higher desorption energy than silica (e.g. Mazeina and Navrotsky, 2007; Sneh et al., 1996). We observe,
- 10 however, that the data does not show the typical multilayer behaviour where coverage increases with saturation. This is a result of the curvature effect, which strongly influences the equilibrium coverage for nanometer-sized particles. Instead, we find that the adsorption model that we used recently (Nachbar et al., 2018a) to describe the water affinity of iron-silicate particles describes the water coverage more adequately. **In this work we modify this model to account for the influence of the curvature on the equilibrium coverage, which has not been done before.**
- 15 The model was originally used to describe the surface concentration of adsorbed monomers at sub-monolayer coverage on a planar surface (Pruppacher and Klett, 2004). It assumes a homogeneous particle surface in which all surface binding sites for adsorbent molecules are characterized by the same surface desorption energy  $E_{\text{des}}^0$ . The equilibrium between desorbing water molecule flux density  $j_{\text{des}}$  and adsorbing flux density  $j_{\text{ads}}$  yields

$$\underbrace{\frac{n \cdot v_{\text{th}}}{4}}_{j_{\text{ads}}} = \underbrace{c \cdot f \cdot \exp\left(-\frac{E_{\text{des}}^0}{RT}\right) \cdot S_K(r_{\text{dry}})}_{j_{\text{des}}} \cdot \quad (3)$$

- 20 Here,  $n$  and  $v_{\text{th}}$  are the number density and the mean thermal velocity of gas phase water molecules, respectively. The number of adsorbed water molecules is described by  $c=m_{\text{ads}}/(m_{\text{H}_2\text{O}} \cdot A_{\text{dry}})$  with the surface area of the dry particle  $A_{\text{dry}}=4\pi r_{\text{dry}}^2$ .

The other parameters are the vibrational frequency  $f=10^{13}$  Hz for H<sub>2</sub>O (Pruppacher and Klett, 2004), the universal gas constant  $R$ , and particle temperature  $T$ . Compared to our previous work (Nachbar et al., 2018a), we added a Kelvin-effect-like term

$$S_K = \exp\left(\frac{2\sigma M}{RT\rho r_{dry}}\right) \quad (4)$$

to the flux density of desorbing molecules in order to take the increased desorption due to the curvature effect into account. Here,  $M$  is the molar mass of water,  $\rho$  is the density of the adsorbed water film which we assume is similar to the density of ice, and  $\sigma$  is the interfacial tension between the water film and air. We do not take into account the influence of the particle charge and of the collision radius of water molecules on the equilibrium saturation. Both effects are small compared to the Kelvin-term and would make the parameterization unnecessarily complicated. Additionally, they would render Eq. (3) analytically not solvable. By neglecting these effects we can re-arrange the equation to yield:

$$\underbrace{RT \cdot \ln\left(\frac{4cf}{nv_{th}}\right)}_{\equiv E_{des}} = E_{des}^0 - \frac{2\sigma M}{\rho} \cdot \frac{1}{r_{dry}}. \quad (5)$$

In Fig. 3 we plot the curvature-dependent desorption energy  $E_{des}$  as defined by the left-hand-side of Eq. (5) versus the inverse of the dry particle radius using measured data for the adsorbed water vapour mass  $m_{ads}$ . From the intercept the curvature-independent desorption energy can be obtained while the slope is directly proportional to the surface tension of the water ad-layer - air interface. The figure shows that the three particle materials exhibit different desorption energies and that the water molecules are on average less strongly bound to the particle surface on smaller particles due to the curvature effect.

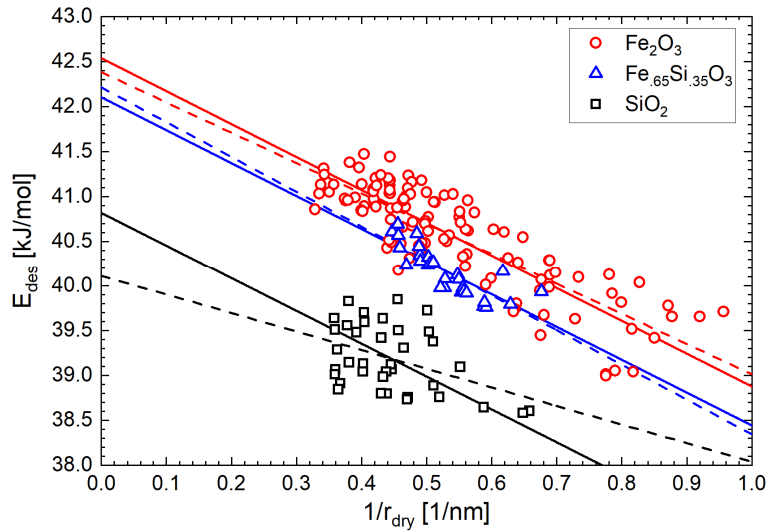
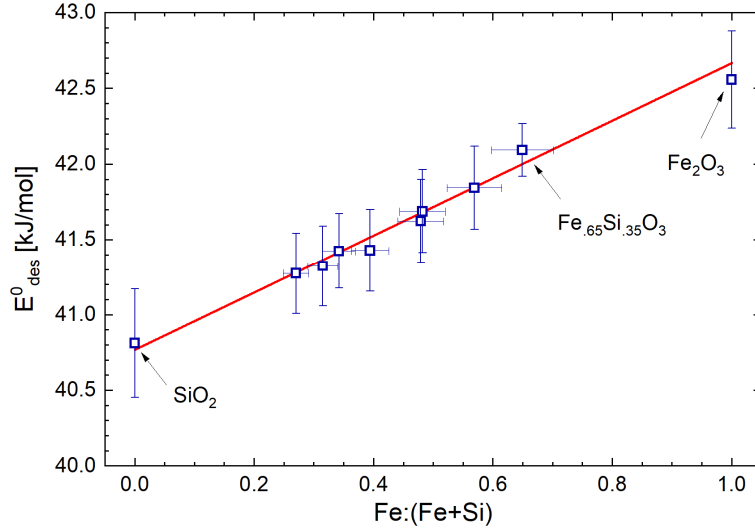


Figure 3. Surface desorption energy of water molecules on iron silicate nanoparticles calculated from measured water coverages using Eq. (5). Dashed lines are independent linear fits and solid lines represent a combined linear fit resulting in  $\sigma=0.094$  Nm<sup>-1</sup>.

In order to determine the surface tension of the water ad-layer we performed independent linear fits to the three data sets which are shown as dashed lines in Fig. 3. The determined surface tensions are  $\sigma(\text{H}_2\text{O-on-Fe}_2\text{O}_3)=(87\pm 5) \text{ mNm}^{-1}$ ,  $\sigma(\text{H}_2\text{O-on-Fe}_{.65}\text{Si}_{.35}\text{O}_3)=(99\pm 13) \text{ mNm}^{-1}$ , and  $\sigma(\text{H}_2\text{O-on-SiO}_2)=(53\pm 18) \text{ mNm}^{-1}$ . To keep the intended parameterization for the water coverage as function of the particle material as simple as possible, we refrained from using a material dependent surface tension of the water ad-layer. We performed a combined fit with a single value for the surface tension for all three materials. The resulting fits yielded  $\sigma=(94\pm 11) \text{ mNm}^{-1}$ , which compares very well to **extrapolated values of** the surface tension of **supercooled liquid water (SLW)** at these temperatures ( $\sigma_{\text{SLW}}(T=155 \text{ K})=92 \text{ mNm}^{-1}$  and  $\sigma_{\text{SLW}}(T=128 \text{ K})=96 \text{ mNm}^{-1}$ ) **which we proposed recently to use for lack of available surface tension data of ASW** (Nachbar et al., 2018c). The **combined fit is** shown as solid lines in Fig. 3. From the intercepts of the linear fits we determined the curvature independent desorption energies  $E^0_{\text{des}}(\text{Fe}_2\text{O}_3)=(42.5\pm 0.3) \text{ kJmol}^{-1}$ ,  $E^0_{\text{des}}(\text{Fe}_{.65}\text{Si}_{.35}\text{O}_3)=(42.1\pm 0.2) \text{ kJmol}^{-1}$ , and  $E^0_{\text{des}}(\text{SiO}_2)=(40.8\pm 0.4) \text{ kJmol}^{-1}$ . We also re-analysed the adsorption data for mixed iron-silicate particles published in Nachbar et al. (2018a) using Eq. (5) and  $\sigma=94 \text{ mNm}^{-1}$ . The resulting curvature independent desorption energies are shown in Fig. 4. Here, the 3 labelled data points are the intercepts from Fig. 3 while all other data points represent single measurements analysed using Eq. (5).



15 **Figure 4. Curvature-independent average desorption energy as function of iron content of iron silicate particles. The red line represents a linear fit to the data. Based in part on original data from Nachbar et al. (2018a).**

The average curvature independent desorption energies follow the linear relation:

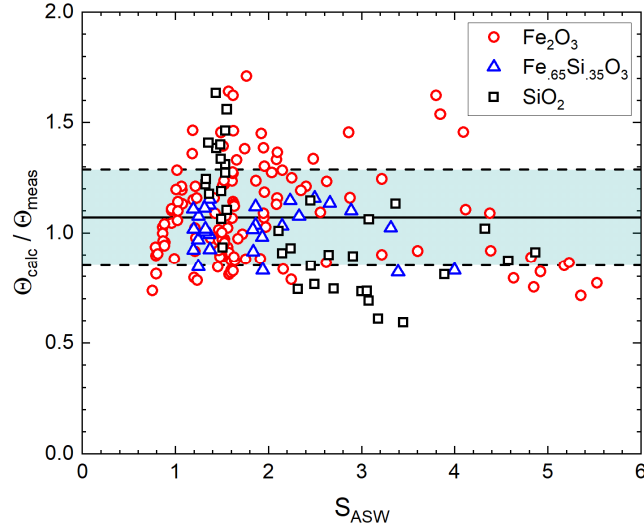
$$E^0_{\text{des}} \left[ \frac{\text{kJ}}{\text{mol}} \right] = (40.8 \pm 0.1) + (1.899 \pm 0.103) \cdot X, \quad (6)$$

where  $X=\text{Fe}/(\text{Fe}+\text{Si})$  represents the relative iron content. Inserting this in Eq. (3) we arrive at a parameterization for the water coverage for iron silicate particles at mesopause conditions

$$m_{\text{ads}} = A_{\text{dry}} m_{\text{H}_2\text{O}} \frac{n \cdot v_{\text{th}}}{4f} \cdot \exp \left( \frac{E^0_{\text{des}}}{RT} - \frac{2\sigma M}{RT \rho r_{\text{dry}}} \right), \quad (7)$$

which can be used to predict the mass of adsorbed water for iron-silicate particles as function of the dry particle radius, temperature and water vapour concentration. The wet particle radius  $r_{wet}$  and the water coverage  $\Theta$  can be calculated from  $m_{ads}$  using:

$$r_{wet}^3 = r_{dry}^3 + \frac{3}{4\pi} \frac{m_{ads}}{\rho}; \quad \Theta = \frac{r_{wet} - r_{dry}}{d_{ML}} \quad (8)$$



5

**Figure 5. Ratio of calculated water coverage using Eq. (7) and measured water coverage as function of the saturation ratio.**

In Fig. 5 we show the ratio of calculated to measured water coverages for all three materials. The average calculated water coverage deviates by about 7% from the measurements (solid line) with a mean square deviation of about 22% (dashed lines). The comparison shows that the measured water coverage is well represented by our water adsorption parameterization for particles between  $r=1-3$  nm and temperatures between 128 and 152 K. Applied water vapour partial pressures range between about  $2 \cdot 10^{-7}$  and  $10^{-4}$  Pa.

10

### 3.2 Critical saturation for ice activation

We have measured the critical saturation for the activation of ice growth on small iron silicate nano-particles ( $r_{dry}=1.05-2.8$  nm) in the temperature interval between 128 and 147 K for three different particle compositions in a total of 53 independent experiments. Figure 6a shows the measured critical saturations as a function of the initial dry particle radius for pure iron oxide ( $Fe_2O_3$ ) particles at four different temperatures. Note that we plot here the saturation ratio with respect to the vapour pressure of hexagonal ice to facilitate comparison with other studies. Figure 6b compares the results at 139.6 K with measurements on silica and one mixed iron-silicate with an elemental ratio  $Fe/(Fe+Si)=0.65$ . Note that in all measurements ice growth is activated below  $S_h=50$ , which compares to observations of saturation ratios exceeding  $S_h=100$  when temperatures drop below 140 K on a regular basis during NLC season (Lübken et al., 2009). The solid lines in Fig. 6 are the results of an adsorption-activation model which we will present below.

15

20

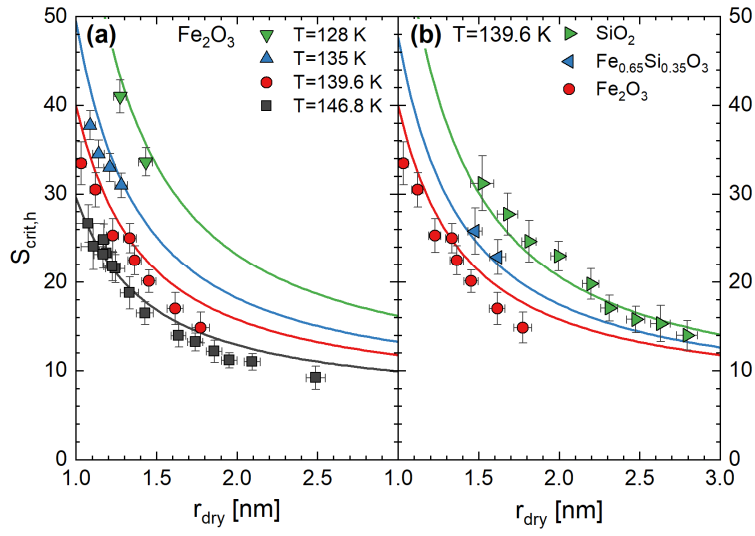


**Figure 6. Critical saturation as function of initial particle radius. Solid lines represent the ice activation model (see text for details).**

We have shown previously that ASW is the initial form of condensed water that deposits on hydrophilic iron silicate nanoparticles at temperatures below 160 K (Nachbar et al., 2018c). It is well known that depending on growth conditions

5 microporous ASW may be formed and that background gas molecules may be trapped during deposition. However, ASW samples produced above 100 K in the absence of a background gas were found to be compact or exhibited the same surface area as crystalline ice reference samples indicating the formation of compact ASW (Mayer and Pletzer, 1986; Stevenson et al., 1999; Westley et al., 1998). We thus argue that at the experimental conditions employed in our study (surface temperature of  $T \geq 128\text{K}$ , maximum deposition rate  $3\text{\AA/s}$  ( $\sim 1\text{ML/s}$ ), Helium as a background gas) compact ASW is created

10 on the nanoparticles with at maximum a marginal degree of porosity. Here, we will rely on a simple approach to describe ice formation in the mesopause by assuming that the nuclei are spherical and perfectly wettable (contact parameter close to one, i.e. the activation barrier to form ASW is low). Under such conditions, and taking into account that the ice particle is charged, ice formation is likely to occur near the equilibrium saturation which is given by the Kelvin-Thomson equation for the particle radius including the adsorbed water  $r_{\text{wet}}$ :

$$15 \quad \ln(S_{KT}) = \frac{M}{RT\rho} \left[ \frac{2\sigma}{r_{\text{wet}}} - \frac{Q^2}{32\pi^2\epsilon_0 r_{\text{wet}}^4} \left( 1 - \frac{1}{\epsilon_r} \right) \right], \quad (9)$$

where  $Q$  is the particle charge, and  $\epsilon_0$  and  $\epsilon_r$  are the permittivity of vacuum and the relative permittivity of water, respectively. Above we showed that the MSP analogues are already covered with more than one monolayer of water at saturations below the ice activation threshold. This water film is well described using bulk properties for the surface tension

of ASW. For the surface tension of ASW we use  $\sigma_{\text{ASW}} = (114.8 - 0.144 \cdot T [\text{K}]) \text{ mN m}^{-1}$ , a parameterization which is based on a low-temperature extrapolation of measured data for supercooled water (Vinš et al., 2017). Our previous study on the vapour pressure of compact ASW indicates that this parameterization is consistent with the properties of ASW to within 10% at the

investigated temperatures between 133 and 147 K (Nachbar et al., 2018c). For the density of compact ASW we use a constant value of  $\rho_{ASW}=0.93 \text{ gcm}^{-3}$  (Brown et al., 1996; Loerting et al., 2011).

In the derivation of the Kelvin-Thomson equation, the vapour in equilibrium with the condensed phase is assumed to be an ideal gas. This also includes the assumption that the gas phase molecules are point-like. This assumption breaks down when the size of the particle becomes comparable to the size of the water molecules. When taking the size of water molecules into account using a hard sphere collision model the equilibrium saturation changes to:

$$S_{KT}^* = S_{KT} \cdot \left(1 + \frac{r_{H_2O}}{r_{wet}}\right)^{-2}. \quad (10)$$

The second term on the right-hand-side represents the correction due to the finite size of the water molecules for which we use  $r_{H_2O}=1.5 \text{ \AA}$  (Bickes et al., 1975). The right-hand side of Eq. (10) reduces to the Kelvin-Thomson term for  $r_{H_2O}/r \ll 1$ . In our adsorption-activation model the onset conditions for ice growth are reached when the saturation in the environment of the particle surpasses the equilibrium saturation given by Eq. (10) ( $S_{ASW} \geq S_{KT}^*$ ). The adsorption-activation model is illustrated in Fig. 7 for  $r_{dry}=2 \text{ nm}$  particles at  $T=140 \text{ K}$ . Here, the Kelvin-Thomson radius  $r_{wet}=f^{-1}(S_{KT}^*)$  represents the boundary between equilibrium and ice growth regime (dash-dotted line). For comparison, we also plotted the Kelvin-Thomson radius where we neglected the  $H_2O$  collision radius (dashed line). Solid lines represent the wet particle radius in equilibrium regime according to Eq. (7) and Eq. (8) for  $Fe_2O_3$  in red and  $SiO_2$  in black. The onset conditions are defined in our model by the saturation ratio  $S_{ASW}$  for which the particle radius in equilibrium regime intersects the Kelvin-Thomson radius.

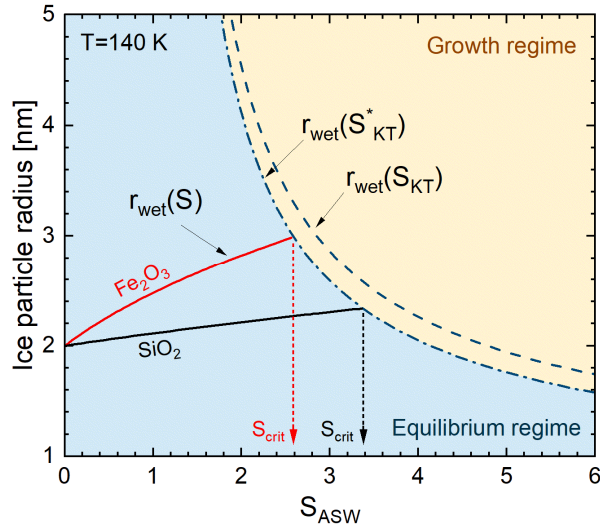
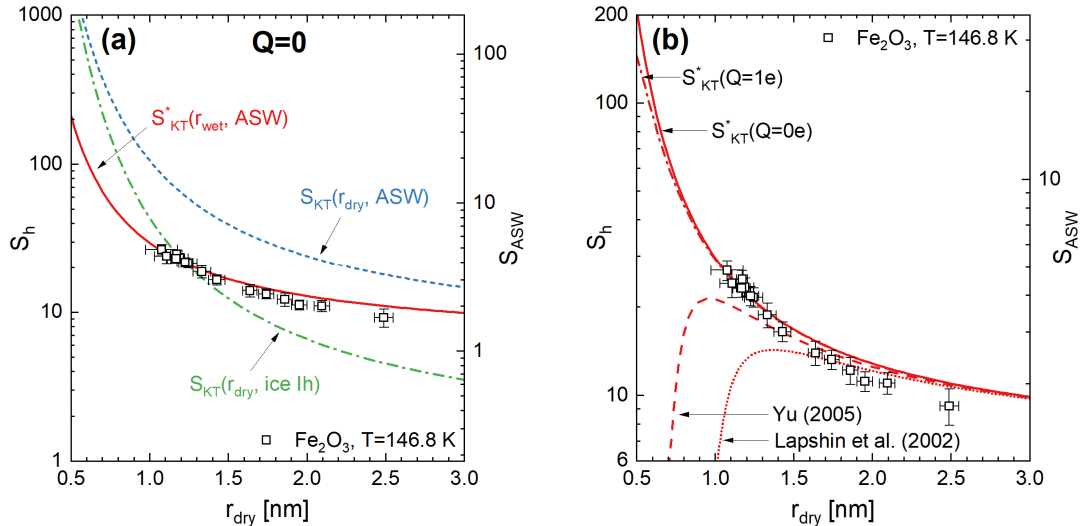


Figure 7. Illustration of the adsorption-activation model. Solid lines represent the wet particle radius in equilibrium regime calculated using Eq. (7) and Eq. (8). Dash-dotted and dashed lines represent the Kelvin-Thomson radius ( $Q=1e$ ) calculated with and without  $H_2O$  collision radius using Eq. (10), respectively.

We determined the critical saturation ratios using this method and plotted the results as solid lines in Fig. 6 for all temperatures and particle compositions shown. The model curves agree well with measured data confirming the method as a good predictor for ice growth onset at mesopause conditions.



5 **Figure 8.** Comparison of measured onset conditions for ice activation for  $\text{Fe}_2\text{O}_3$  particles at  $T=146.8$  K with different model calculations. Panel a) Comparison of the **critical** saturation given by the activation model excluding charge effects (Eq. 9,  $Q=0e$ ). The red solid line represents calculations using the wet particle radius while the blue dashed and green dash-dotted lines represent calculations using the dry particle radius assuming **compact** ASW and hexagonal ice, respectively. Panel b) Comparison of the activation model for charged (dash-dotted line,  $Q=1e$ ) and neutral (solid line,  $Q=0e$ ) particles. **The dotted and dashed lines show the ice activation model using modified versions of the Kelvin-Thomson equation** (see text for details).  
 10

In Fig. 8a we plot the results of the adsorption-activation model (solid red curve) for iron oxide particles at 146.8 K. The blue dashed line was calculated using the adsorption activation model but assuming that no water adsorbs prior to activation. The comparison of both model calculations shows that the equilibrium saturation is substantially reduced due to the adsorption of several monolayers of water near the activation threshold. Also shown as a green dash-dotted line is the activation model assuming the formation of hexagonal ice and assuming that no water adsorbs prior to activation. These calculations represent the lowest critical saturations currently assumed in mesospheric models (e.g. Berger and Lübken, 2015; Schmidt et al., 2018). However, it is expected that the majority of MSPs in the mesopause is smaller than  $r=1.2$  nm (Bardeen et al., 2008; Megner et al., 2008a; Megner et al., 2008b; Plane et al., 2014). Ice formation on such small particles has to occur in order to explain observed ice particle concentrations in PMCs. According to our activation model, critical saturations are substantially smaller than currently assumed for particles with  $r < 1.2$  nm.  
 15  
 20

Figure 8b compares the **critical** saturation predicted by the activation model for neutral particles (solid curve) with singly charged particles (dash-dotted curve). We note that the presence of several monolayers of water substantially increases the particle radius at the activation threshold which effectively decreases the influence of the particle charge. In **our ice activation model**, the particle charge becomes significant only below  $r_{\text{dry}}=0.6$  nm. Note that such small iron oxide particles only consist of about 90 atoms. In Fig. 8b **we also plot the critical saturation using modified versions of the Kelvin-Thomson**  
 25

equation according to Yu (2005) and Lapshin et al. (2002), which are in disagreement with our measurements below  $r_{\text{dry}}=1.2$  nm.

#### 4 Conclusions

We measured the critical saturation for ice growth on iron-silicate nano-particles serving as meteor smoke substitutes under conditions of PMC formation. Our results show that for iron-silicate particles of dry particle radius  $r=1$  nm and above ice growth initiates below  $S_h=50$  which is commonly exceeded during NLC season. This affirms meteoric smoke particles as likely nuclei for heterogeneous ice formation in mesospheric clouds. The onset conditions for ice activation for iron oxide, silica and iron-silicates are well represented by the reduced equilibrium saturation of the wet particle radius using the saturation vapour pressure and surface tension of ASW. This confirms our hypothesis of ASW activation and is in line with our previous observation of ASW depositional growth at mesopause conditions (Nachbar et al., 2018c). The activation threshold can be matched even more precisely by taking into account the collision radius of water molecules. Based on the ice activation model we showed that due to the adsorbed water layer, charge effects play only a minor role in the ice activation of iron-silicate particles larger than a dry size of  $r=0.6$  nm. For smaller nano-particles and clusters other competing effects may come into play which could potentially influence the equilibrium saturation, for instance the curvature dependence of the surface tension (Tolman, 1949), or long-range interactions between droplet surface and water molecules (Park et al., 2016; Vasil'ev and Reiss, 1996a, b). Our findings are parameterized in Eqs. (6), (7), and (10) which yield the wet particle diameter and ice cloud activation threshold as a function of humidity, temperature, dry particle size and iron content. Our results support our previous finding that amorphous solid water has to be considered as a relevant ice polymorph in polar mesospheric cloud formation.

During the summer season, iron rich particles are heated by absorbed sunlight and it was argued that this would modify their ice activation potential. In an accompanying article (Nachbar et al., 2018d) we show that this is a minor effect under typical mesospheric conditions.

#### Author contribution

DD, MN and TL designed the research, MN and DD performed the measurements and analyzed the data. DD wrote the manuscript with contributions by the co-authors. TL supervised the project.

#### Competing interests

The authors declare that they have no conflict of interest.

## Acknowledgements

The authors thank the German Federal Ministry of Education and Research (BMBF, grant number 05K13VH3 and 05K16VHB) and the German Research Foundation (DFG, grant number LE 834/4-1) for financial support of this work. We acknowledge support by the Deutsche Forschungsgemeinschaft and Open Access Publishing Fund of Karlsruhe Institute of Technology.

## References

- Bardeen, C. G., Toon, O. B., Jensen, E. J., Marsh, D. R., and Harvey, V. L.: Numerical simulations of the three-dimensional distribution of meteoric dust in the mesosphere and upper stratosphere, *J. Geophys. Res. Atmos.*, 113, 2008.
- Berger, U. and Lübken, F.-J.: Trends in mesospheric ice layers in the Northern Hemisphere during 1961–2013, *J. Geophys. Res. Atmos.*, 120, 11277-11298, 2015.
- Bickes, R. W., Duquette, G., van den Meijdenberg, C. J. N., Rulis, A. M., Scoles, G., and Smith, K. M.: Molecular Beam Scattering Experiments with Polar Molecules: Measurement of Differential Collision Cross Sections for H<sub>2</sub>O+H<sub>2</sub>, He, Ne, Ar, H<sub>2</sub>O and NH<sub>3</sub>+H<sub>2</sub>, He, NH<sub>3</sub>, *J. Phys. B*, 8, 3034-3043, 1975.
- Brown, D. E., George, S. M., Huang, C., Wong, E. K. L., Rider, K. B., Smith, R. S., and Kay, B. D.: H<sub>2</sub>O Condensation Coefficient and Refractive Index for Vapor-Deposited Ice from Molecular Beam and Optical Interference Measurements, *J. Phys. Chem.*, 100, 4988-4995, 1996.
- Carrillo-Sánchez, J. D., Nesvorný, D., Pokorný, P., Janches, D., and Plane, J. M. C.: Sources of cosmic dust in the Earth's atmosphere, *Geophys. Res. Lett.*, 43, 11979-11986, 2016.
- DeLand, M. T., Shettle, E. P., Thomas, G. E., and Olivero, J. J.: Latitude-dependent long-term variations in polar mesospheric clouds from SBUV version 3 PMC data, *J. Geophys. Res. Atmos.*, 112, 2007.
- Demissie, T. D., Espy, P. J., Kleinknecht, N. H., Hatlen, M., Kaifler, N., and Baumgarten, G.: Characteristics and sources of gravity waves observed in noctilucent cloud over Norway, *Atmos. Chem. Phys.*, 14, 12133-12142, 2014.
- Duft, D., Nachbar, M., Eritt, M., and Leisner, T.: A Linear Trap for Studying the Interaction of Nanoparticles with Supersaturated Vapors, *Aerosol Sci. Tech.*, 49, 683-691, 2015.
- Gumbel, J. and Megner, L.: Charged meteoric smoke as ice nuclei in the mesosphere: Part 1-A review of basic concepts, *J. Atmos. Sol.-Terr. Phys.*, 71, 1225-1235, 2009.
- Hervig, M. E., Berger, U., and Siskind, D. E.: Decadal variability in PMCs and implications for changing temperature and water vapor in the upper mesosphere, *J. Geophys. Res. Atmos.*, 121, 2383-2392, 2016.
- Hervig, M. E., Brooke, J. S. A., Feng, W., Bardeen, C. G., and Plane, J. M. C.: Constraints on Meteoric Smoke Composition and Meteoric Influx Using SOFIE Observations With Models, *J. Geophys. Res. Atmos.*, 122, 13495-13505, 2017.
- Hervig, M. E., Stevens, M. H., Gordley, L. L., Deaver, L. E., Russell, J. M., and Bailey, S. M.: Relationships between polar mesospheric clouds, temperature, and water vapor from Solar Occultation for Ice Experiment (SOFIE) observations, *J. Geophys. Res. Atmos.*, 114, 2009.
- Kaifler, N., Baumgarten, G., Fiedler, J., and Lübken, F. J.: Quantification of waves in lidar observations of noctilucent clouds at scales from seconds to minutes, *Atmos. Chem. Phys.*, 13, 11757-11768, 2013.
- Keese, R. G.: Nucleation and Particle Formation in the Upper Atmosphere, *J. Geophys. Res. Atmos.*, 94, 14683-14692, 1989.

- Kirkwood, S., Dalin, P., and Réchou, A.: Noctilucent clouds observed from the UK and Denmark & trends and variations over 43 years, *Ann. Geophys.*, 26, 1243-1254, 2008.
- Lapshin, V. B., Yablokov, M. Y., and Palei, A. A.: Vapor pressure over a charged drop, *Russ. J. Phys. Chem.*, 76, 1727-1729, 2002.
- 5 Leslie, R. C.: Sky Glows, *Nature*, 32, 245, 1885.
- Loerting, T., Bauer, M., Kohl, I., Watschinger, K., Winkel, K., and Mayer, E.: Cryoflotation: Densities of Amorphous and Crystalline Ices, *J. Phys. Chem. B*, 115, 14167-14175, 2011.
- Lübken, F. J., Lautenbach, J., Höffner, J., Rapp, M., and Zecha, M.: First continuous temperature measurements within polar mesosphere summer echoes, *J. Atmos. Sol.-Terr. Phys.*, 71, 453-463, 2009.
- 10 Mayer, E. and Pletzer, R.: Astrophysical implications of amorphous ice - a microporous solid, *Nature*, 319, 298-301, 1986.
- Mazeina, L. and Navrotsky, A.: Enthalpy of Water Adsorption and Surface Enthalpy of Goethite ( $\alpha$ -FeOOH) and Hematite ( $\alpha$ -Fe<sub>2</sub>O<sub>3</sub>), *Chem. Mater.*, 19, 825-833, 2007.
- Megner, L., Gumbel, J., Rapp, M., and Siskind, D. E.: Reduced meteoric smoke particle density at the summer pole – Implications for mesospheric ice particle nucleation, *Adv. Space Res.*, 41, 41-49, 2008a.
- 15 Megner, L., Siskind, D. E., Rapp, M., and Gumbel, J.: Global and temporal distribution of meteoric smoke: A two-dimensional simulation study, *J. Geophys. Res. Atmos.*, 113, 2008b.
- Meinen, J., Khasminskaya, S., Ruehl, E., Baumann, W., and Leisner, T.: The TRAPS Apparatus: Enhancing Target Density of Nanoparticle Beams in Vacuum for X-ray and Optical Spectroscopy, *Aerosol Sci. Tech.*, 44, 316-328, 2010.
- Murphy, D. M. and Koop, T.: Review of the vapour pressures of ice and supercooled water for atmospheric applications, *Q. J. R. Meteorol. Soc.*, 131, 1539-1565, 2005.
- 20 Nachbar, M., Duft, D., Kiselev, A., and Leisner, T.: Composition, Mixing State and Water Affinity of Meteoric Smoke Analogue Nanoparticles Produced in a Non-Thermal Microwave Plasma Source, *Z. Phys. Chem.*, 232, 635-648, 2018a.
- Nachbar, M., Duft, D., and Leisner, T.: The vapour pressure over nano-crystalline ice, *Atmos. Chem. Phys.*, 18, 3419-3431, 2018b.
- 25 Nachbar, M., Duft, D., and Leisner, T.: Volatility of Amorphous Solid Water, *J. Phys. Chem. B*, 122, 10044-10050, 2018c.
- Nachbar, M., Duft, D., Mangan, T. P., Martin, J. C. G., Plane, J. M. C., and Leisner, T.: Laboratory measurements of heterogeneous CO<sub>2</sub> ice nucleation on nanoparticles under conditions relevant to the Martian mesosphere, *J. Geophys. Res. Planets*, 121, 753-769, 2016.
- Nachbar, M., Wilms, H., Duft, D., Aylett, T., Kitajima, K., Majima, T., Plane, J. M. C., Rapp, M., and Leisner, T.: The impact of solar radiation on polar mesospheric ice particle formation, *Atmos. Chem. Phys. Discuss.*, 2018, 1--13, 2018d.
- 30 Navrotsky, A., Mazeina, L., and Majzlan, J.: Size-Driven Structural and Thermodynamic Complexity in Iron Oxides, *Science*, 319, 1635, 2008.
- Park, Y., Tanimura, S., and Wyslouzil, B. E.: Enhanced growth rates of nanodroplets in the free molecular regime: The role of long-range interactions, *Aerosol Sci. Tech.*, 50, 773-780, 2016.
- 35 Plane, J. M. C., Feng, W., and Dawkins, E. C. M.: The Mesosphere and Metals: Chemistry and Changes, *Chem. Rev.*, 115, 4497-4541, 2015.
- Plane, J. M. C., Saunders, R. W., Hedin, J., Stegman, J., Khaplanov, M., Gumbel, J., Lynch, K. A., Bracikowski, P. J., Gelinas, L. J., Friedrich, M., Blindheim, S., Gausa, M., and Williams, B. P.: A combined rocket-borne and ground-

- based study of the sodium layer and charged dust in the upper mesosphere, *J. Atmos. Sol.-Terr. Phys.*, 118, 151-160, 2014.
- Pruppacher, H. R. and Klett, J. D.: *Microphysics of Clouds and Precipitation*, Kluwer Academic Publishers, Dordrecht, 2004.
- 5 Rapp, M., Lübken, F. J., Müllemann, A., Thomas, G. E., and Jensen, E. J.: Small-scale temperature variations in the vicinity of NLC: Experimental and model results, *J. Geophys. Res. Atmos.*, 107, 2002.
- Rapp, M., Plane, J. M. C., Strelnikov, B., Stober, G., Ernst, S., Hedin, J., Friedrich, M., and Hoppe, U. P.: In situ observations of meteor smoke particles (MSP) during the Geminids 2010: constraints on MSP size, work function and composition, *Ann. Geophys.*, 30, 1661-1673, 2012.
- 10 Rapp, M. and Thomas, G. E.: Modeling the microphysics of mesospheric ice particles: Assessment of current capabilities and basic sensitivities, *J. Atmos. Sol.-Terr. Phys.*, 68, 715-744, 2006.
- Rong, P. P., Yue, J., Russell, J. M., Lumpe, J. D., Gong, J., Wu, D. L., and Randall, C. E.: Horizontal winds derived from the polar mesospheric cloud images as observed by the CIPS instrument on the AIM satellite, *J. Geophys. Res. Atmos.*, 120, 5564-5584, 2015.
- 15 Schmidt, F., Baumgarten, G., Berger, U., Fiedler, J., and Lübken, F. J.: Local time dependence of polar mesospheric clouds: a model study, *Atmos. Chem. Phys.*, 18, 8893-8908, 2018.
- Seele, C. and Hartogh, P.: Water vapor of the polar middle atmosphere: Annual variation and summer mesosphere Conditions as observed by ground-based microwave spectroscopy, *Geophys. Res. Lett.*, 26, 1517-1520, 1999.
- Sneh, O., Cameron, M. A., and George, S. M.: Adsorption and desorption kinetics of H<sub>2</sub>O on a fully hydroxylated SiO<sub>2</sub> surface, *Surf. Sci.*, 364, 61-78, 1996.
- 20 Stevenson, K. P., Kimmel, G. A., Dohnalek, Z., Smith, R. S., and Kay, B. D.: Controlling the morphology of amorphous solid water, *Science*, 283, 1505-1507, 1999.
- Thomas, G. E.: Mesospheric clouds and the physics of the mesopause region, *Rev. Geophys.*, 29, 553-575, 1991.
- Thomas, G. E. and Olivero, J.: Noctilucent clouds as possible indicators of global change in the mesosphere, *Adv. Space Res.*, 28, 937-946, 2001.
- 25 Tolman, R. C.: The Effect of Droplet Size on Surface Tension, *J. Chem. Phys.*, 17, 333-337, 1949.
- Vasil'ev, O. V. and Reiss, H.: Capture of vapor molecules by a realistic attraction potential of a drop, *J. Chem. Phys.*, 105, 2946-2947, 1996a.
- Vasil'ev, O. V. and Reiss, H.: Effect of the attractive potential of a drop in vapor phase nucleation, *Phys. Rev. E*, 54, 3950-3954, 1996b.
- 30 Venables, J. A., Spiller, G. D. T., and Hanbucken, M.: Nucleation and growth of thin films, *Rep. Prog. Phys.*, 47, 399, 1984.
- Vinš, V., Hošek, J., Hykl, J., and Hrubý, J.: Surface Tension of Supercooled Water: Inflection Point-Free Course down to 250 K Confirmed Using a Horizontal Capillary Tube, *J. Chem. Eng. Data*, 62, 3823-3832, 2017.
- Vondrak, T., Plane, J. M. C., Broadley, S., and Janches, D.: A chemical model of meteoric ablation, *Atmos. Chem. Phys.*, 8, 7015-7031, 2008.
- 35 Westley, M. S., Baratta, G. A., and Baragiola, R. A.: Density and index of refraction of water ice films vapor deposited at low temperatures, *J. Chem. Phys.*, 108, 3321-3326, 1998.
- Yu, F.: Modified Kelvin–Thomson equation considering ion-dipole interaction: Comparison with observed ion-clustering enthalpies and entropies, *J. Chem. Phys.*, 122, 084503, 2005.
- 40